Calving and ice-shelf break-up processes investigated by proxy: Antarctic tabular iceberg evolution during northward drift

T. SCAMBOS,[1] R. ROSS,[2] R. BAUER,[1] Y. YERMOLIN,[3] P. SKVARCA,[3] D. LONG,[4] J. BOHLANDER,[1] T. HARAN[1]

[1]*National Snow and Ice Data Center, University of Colorado, 1540 30th Street, Boulder, Colorado 80309-0449, USA*
E-mail: teds@nsidc.org
[2]*Avega Systems, 59 Victoria Street, McMahons Point, Sydney, New South Wales 2060, Australia*
[3]*División Glaciología, Instituto Antártico Argentino, Cerrito 1248, C1010AAZ Buenos Aires, Argentina*
[4]*Department of Electrical Engineering, Brigham Young University, 459 Clyde Building, PO Box 24009, Provo, Utah 84602-4099, USA*

ABSTRACT. Using a combination of satellite sensors, field measurements and satellite-uplinked in situ observing stations, we examine the evolution of several large icebergs drifting east of the Antarctic Peninsula towards South Georgia Island. Three styles of calving are observed during drift: 'rift calvings', 'edge wasting' and 'rapid disintegration'. Rift calvings exploit large pre-existing fractures generated in the shelf environment and can occur at any stage of drift. Edge wasting is calving of the iceberg perimeter by numerous small edge-parallel, sliver-shaped icebergs, preserving the general shape of the main iceberg as it shrinks. This process is observed only in areas north of the sea-ice edge. Rapid disintegration, where numerous small calvings occur in rapid succession, is consistently associated with indications of surface melt saturation (surface lakes, firn-pit ponding). Freeboard measurements by ICESat indicate substantial increases in ice-thinning rates north of the sea-ice edge (from $<10 \, \mathrm{m \, a^{-1}}$ to $>30 \, \mathrm{m \, a^{-1}}$), but surface densification is shown to be an important correction ($>2 \, \mathrm{m}$ freeboard loss before the firn saturates). Edge wasting of icebergs in 'warm' surface water (sea-ice-free, $>-1.8°C$) implies a mechanism based on waterline erosion. Rapid disintegration ('Larsen B-style' break-up) is likely due to the effects of surface or saturated-firn water acting on pre-existing crevasses, or on wave- or tidally induced fractures. Changes in microwave backscatter of iceberg firn as icebergs drift into warmer climate and experience increased surface melt suggest a means of predicting when floating ice plates are evolving towards disintegration.

INTRODUCTION

Tabular icebergs calving from the Antarctic coastline undergo a rapid 'climate change' as they drift into warmer air and water in the Southern Ocean. Icebergs are governed by many of the same physical interactions with air and ocean as ice shelves or ice tongues, and thus mimic important ice-shelf processes as they evolve. Moreover, icebergs provide more frequent 'natural experiments' on the effects of warming on floating ice plates, and drifting icebergs experience more rapid warming and much faster evolution than climate-driven shelf areas. We conducted this study to test via observation various concepts for ice-shelf break-up and retreat.

The motivation for understanding ice-plate evolution in warming conditions stems from the importance of ice shelves to the mass balance of ice sheets. A host of recent observations and model studies have shown that ice shelves and ice tongues exert significant control on the glaciers that feed them (Rott and others, 2002; Joughin and others, 2004; Thomas, 2004; Howat and others, 2007). Deep-draft glaciers flowing into areas formerly fronted by thick floating ice consistently show thinning and rapid increases in speed, by factors of 1.5 to ~8, after the removal of the floating ice (Rignot and others, 2004; Scambos and others, 2004), thereby significantly changing the mass balance of the grounded ice. Warming of ocean water and increased surface melting from warmer summer air are clearly responsible for the ice-plate retreats, but several mechanisms have been invoked to explain the process. Among these are: reduced fracture

toughness of near-surface temperate ice (e.g. Vaughan and Doake, 1996); thinning and warming of the ice by surface melt (Rott and others, 1998); stress-field changes arising from changes in ice-front configuration during retreat (Doake and others, 1998); meltwater-driven fracturing of the ice (Scambos and others, 2000, 2003, based on, e.g., Weertman, 1973); within-shelf toppling of rifted ice blocks (MacAyeal and others, 2003); thinning by basal melting (Shepherd and others, 2003); and, potentially, break-up due to long-period waves (MacAyeal and others, 2006; Squire, 2007). However, shelf break-up events are relatively infrequent, and climate-driven evolution of ice shelves requires years to decades to develop.

One type of data largely missing from past studies of ice-shelf, ice-tongue or iceberg response to air and ocean warming is in situ continuous observations. For this study, we developed a remote robotic camera and sensor system, with data uplinked via digital satellite telephone. This system is based on an earlier version used for observing ice-shelf rifts and iceberg drift near the Ross Ice Shelf (Ross and others, 2004).

This study reports on the drift and surface physical characteristics derived from in situ and satellite geophysical observations of two tabular icebergs derived from the Ronne Ice Shelf front and southern Larsen C ice shelf as they drifted north to the region of South Georgia Island. The icebergs are A22A, initially 60 by 40 km in size, and UK211, initially 12 by 10 km (which we have informally named 'Amigosberg' after the monitoring device described below). We
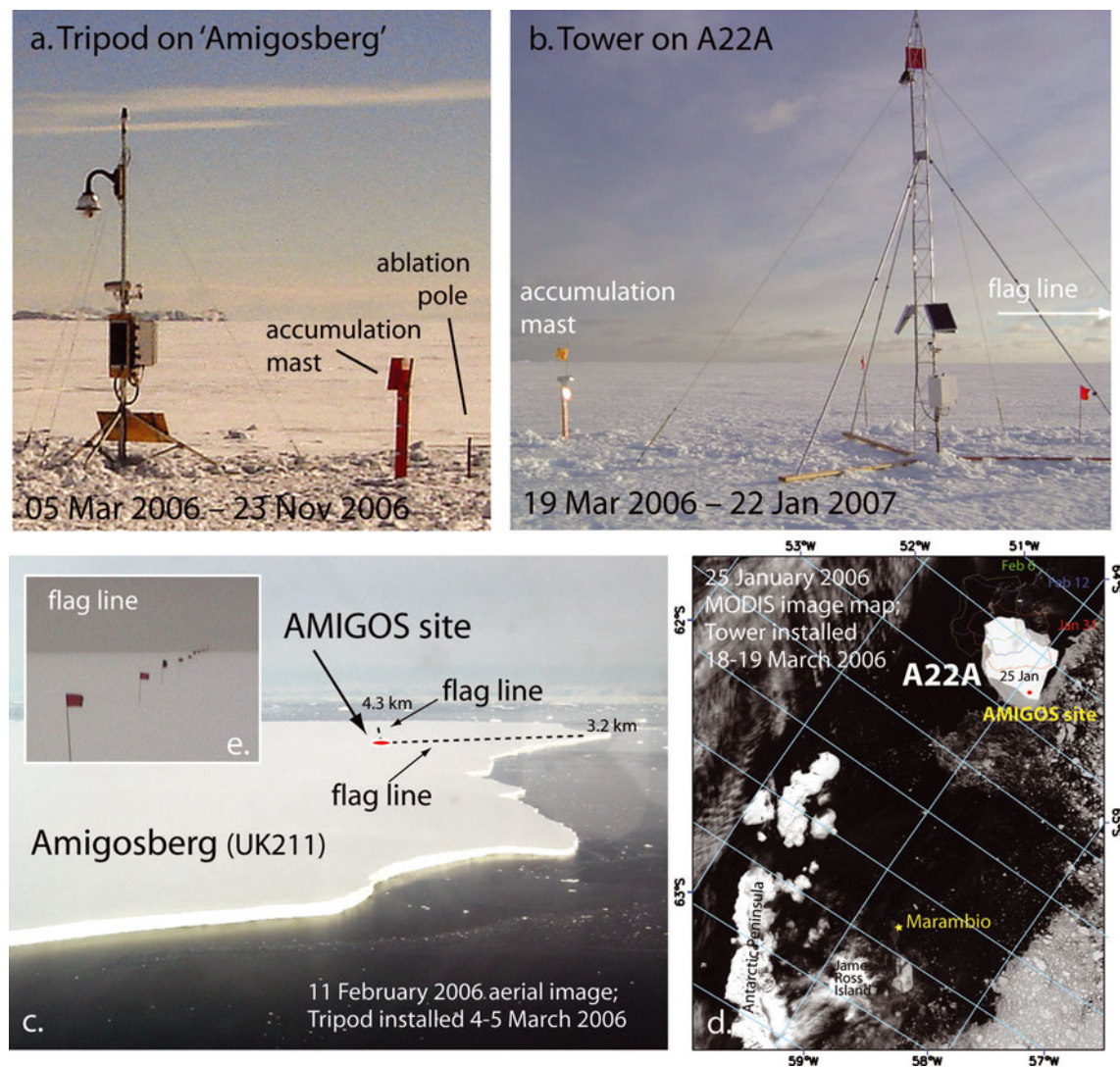
Fig. 1. (a, b) Automated Met-Ice-Geophysics Observation Stations (AMIGOS) were installed on the two primary study icebergs, 'Amigosberg' (UK211) and A22A. The images show configuration of the stations, accumulation masts, flag lines and ablation poles. The dates give the periods of operation of the two stations. (c) Aerial photo of Amigosberg, with overlay showing installation site and distance from ice edges. (d) Image map from MODIS scene showing regional view and site location of AMIGOS site on A22A. (e) Image from Amigosberg site showing one of the flag lines used for flexure observations and edge-wasting monitoring.

supplement our analysis of these two icebergs with additional remote-sensing data from four other icebergs, described in Scambos and others (2005), and numerous smaller icebergs near Marambio station in the Antarctic Peninsula. Using this combination of in situ data and remote sensing, particularly at the late stages of iceberg break-up, we hope to identify details of the break-up processes behind ice-shelf retreat and disintegration.

METHODS

Satellite sensor observations

We used a series of scenes from the moderate-resolution imaging spectroradiometer (MODIS) sensor, combining the visible and near-infrared channels (bands 1–4 of the sensor) at a nominal resolution of 250 m (red and near-infrared) or 500 m (blue and green). These images, and associated geolocation processing, provided information on iceberg location, area and shape, calving events, and changes in surface characteristics. Images with sufficient clear-sky visibility to provide position and shape data were available

about twice per week. Many of the images are archived at the ice-shelf monitoring website at the US National Snow and Ice Data Center (NSIDC; http://nsidc.org/data/iceshelves_images) and are available to the public. Scenes in this archive are projected to polar stereographic and Lambert Conformal Conic projections using the NSIDC MODIS Swath-to-Grid Toolbox software (MS2GT; see Haran and others, 2002; http://nsidc.org/data/modis/ms2gt). Iceberg edges are digitized from the images to determine perimeter and area. Additional iceberg locations are provided by the Antarctic Iceberg Tracking Database using the QuikSCAT Ku-band scatterometer on the SeaWinds satellite (http://www.scp.byu.edu/data/iceberg). These positions are supplemented by two in situ global positioning system (GPS) datasets from automated iceberg-observing stations described below. The QuikSCAT archive also provides scatterometry data in the Ku band (13.6 GHz frequency) at improved spatial resolution via scatterometry image enhancement processing (Early and Long, 2001). Scatterometry changes indicate changes in iceberg surface properties (melt, recent snowfall) as the icebergs evolve. Additional data on iceberg movement,

based on numerous satellite sources, are available from the US National Ice Center (http://www.natice.noaa.gov). Elevation (freeboard) data for the A22A iceberg come from the Ice, Cloud and land Elevation Satellite (ICESat) laser altimeter, which acquires profiles of precise (±20 cm) elevations as a series of ~70 m diameter surface spots spaced 172 m apart. No ICESat tracks were found that crossed the Amigosberg iceberg.

Airborne and space station hand-held camera observations

Additional observations were made during overflights, by aircraft and helicopter, of numerous icebergs near the Argentine Antarctic base Marambio, and from the Argentine Navy icebreaker ARA *Almirante Irizar*. Low-level surveys of ice edges were conducted to observe and photograph fracturing, edge character, melt layering and approximate freeboard height prior to landings on three icebergs (Amigosberg, A22A and an unnamed small iceberg just east of Marambio).

After the field season, further photographs of A22A were acquired from the International Space Station (ISS) by request to the Gateway to Astronaut Photography of Earth program (http://eol.jsc.nasa.gov), showing details at far higher resolution than is available from MODIS images. Hand-held astronaut photography is very effective for moving, fast-changing targets such as drifting icebergs, but lacks precise geolocation or calibration. Nevertheless, important process observations were made using the images.

Field observations and in situ automated stations

During brief (~20 hour) field visits to Amigosberg and A22A, we installed two automated data collection systems, which we call Automated Met-Ice-Geophysics Observation Systems (AMIGOS; Fig. 1). Installation sites were a few kilometers from the iceberg edges to facilitate observations of edge flexure and calving. The units consist of a Linux CPU board and local area network system, with an Iridium digital satellite telephone uplink. The system is powered by rechargeable 100 A-h batteries (two or three) and 20 W solar panels (two or three). Instruments for scientific measurement include a coarse/acquisition code GPS receiver (~3 m precision, latitude and longitude only), air-temperature thermometer, a steerable digital camera and, on one of the stations, an ice-thickness measurement system based on a simple radio-echo sounder. Unfortunately, despite extensive post-processing, we were unable to extract reliable ice-thickness data from the A22A radio-echo sounder unit. Although the unit tested successfully on a smaller iceberg near Marambio, the large metal tower and other objects near the A22A AMIGOS installation interfered with the radio-echo sounder system.

Quantitative measurements by the camera system for other parameters (accumulation, ablation, surface changes and melt) were accomplished by placing pre-marked poles within the field of view. A 1.5 m accumulation mast extending 1 m above the surface was marked with high-contrast reflective tape at 25 cm intervals (Fig. 1b); similarly, two taped bamboo poles (25 cm intervals) were buried to 2.75 m depth for ablation measurements. Accumulation/ablation levels were determined daily from uplinked images (when clear images could be acquired) to within 5 cm. Flagged lines of bamboo poles extending away from the camera towards the ice edges were arranged so that iceberg flexure
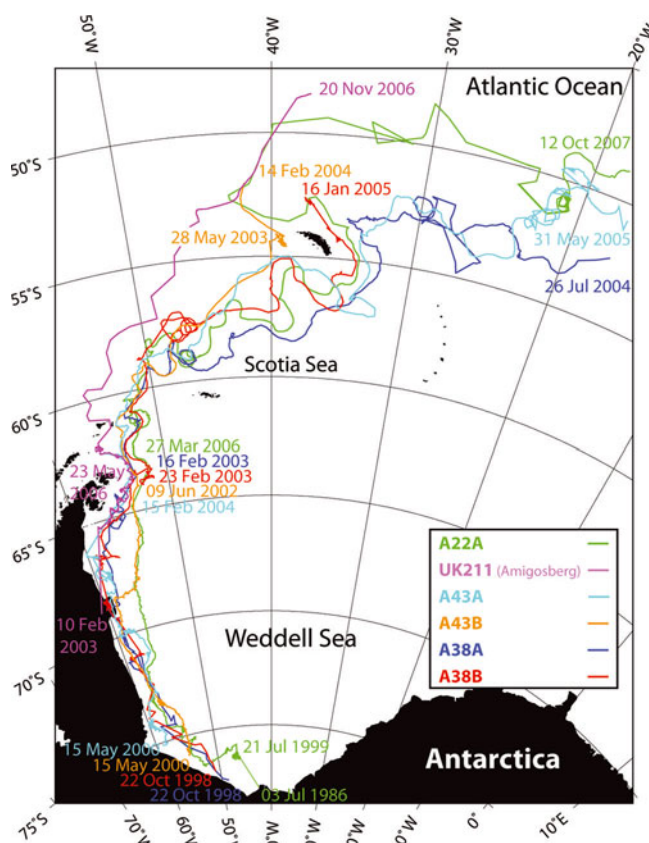

Fig. 2. Map of the drift tracks of the main large icebergs studied here. Dates of initial calving, passage north of ~63° S (northern tip of the Peninsula, and the typical sea-ice edge) and date of last position shown are given. The start date of a prolonged grounding of A43B is also shown.

and edge calvings could be observed and estimated (Fig. 1e). While the AMIGOS units were staked and constructed to withstand high winds and melting, both units tipped over as conditions warmed. However, they continued to operate until, judging from the uplinked images and satellite observations, they fell into the ocean. In both cases, this occurred north of 60° S.

In addition to the installation of AMIGOS units, the field visits included several observations of the iceberg margins, surface structures, snow-pit measurements of density, and firn-core measurements of temperature and structure. Firn density on A22A was measured by a box sampler and a weight scale. Firn temperature on A22A was measured by a hand-held thermometer inserted into the firn-core center immediately after extraction, and reading after 2 min.

OBSERVATIONS

Iceberg movement: QuikSCAT, MODIS and GPS tracking

Iceberg drift tracks follow quasi-predictable routes, with consistent influences from near-stationary gyres, and regions where subsurface currents and ocean shelf slope align the drift paths. Figures 2 and 3 illustrate the large-scale drift of the icebergs, combining approximately twice-weekly QuikSCAT and MODIS image locations for all studied icebergs with hourly GPS positions for the two icebergs carrying AMIGOS systems during their operation period. In
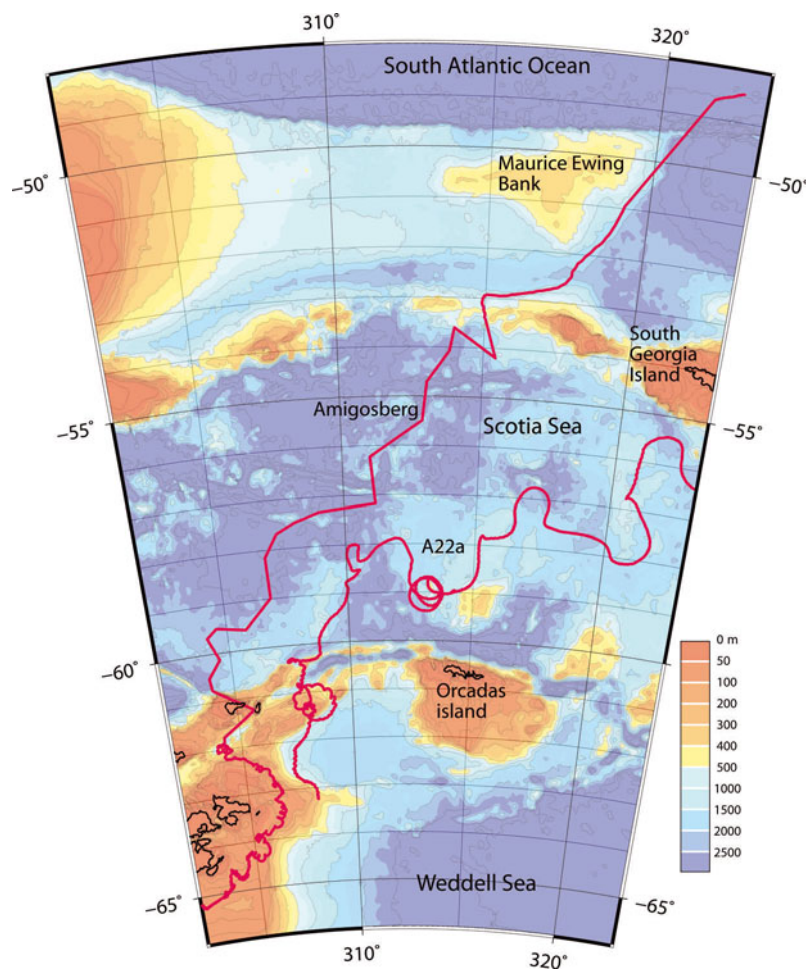
Fig. 3. Bathymetry of the southern Atlantic and Southern Ocean near the Antarctic Peninsula and South Georgia Island. Position tracks for Amigosberg and A22A iceberg are shown. This graphic was created using Generic Mapping Tools (GMT).

Figure 3, the drift tracks for the two AMIGOS unit icebergs, having some GPS hourly positioning, are shown over bathymetry for the Weddell Sea–Scotia Sea–southern Atlantic Ocean.

The general trend of motion in the Weddell Sea–Scotia Sea–South Georgia Island region is a clockwise drift, closely following the eastern continental shelf edge of the Antarctic Peninsula, and then proceeding northeastward towards South Georgia Island (Wordie and Kemp, 1944; Swithinbank and others, 1977; Ferrigno and Gould, 1987; Gladstone and Bigg, 2002; http://www.scp.byu.edu/data/iceberg/database1.html). Large icebergs generally track north of Orcadas island (Laurie Island), and most pass south and east of South Georgia Island, although two of the six studied here drifted west of the island (A43B and Amigosberg). Average net drift speeds (averaging scale of ∼10 days, i.e. removing daily tidal variations) vary greatly, depending on shoal or gyre interactions, but in free-drifting periods the icebergs show a net movement of approximately 2–3 km d^{-1} south of 65°S, 3–5 km d^{-1} between 65°S and 60°S through the Scotia Sea, and 5–15 km d^{-1} in the southernmost South Atlantic (north of 60°S). In the areas nearest the Antarctic mainland, icebergs can move very slowly, and can spend several years on shallow shoals. Indeed, iceberg A22A originally calved from the western Filchner Ice Shelf in 1986 (Skvarca and Garcia, 1993, their '1986C' iceberg).

Several of the study icebergs have nearly overlapping drift tracks for distances of hundreds of kilometers. In the vicinity

of the eastern Peninsula continental shelf, this repetition is apparently due to interaction of regional currents with ocean shelf topography. Shoal isobaths in the drift areas range between 300 and 1000 m. Iceberg drift tracks appear to be separated on the basis of iceberg thickness within these shoal-aligned currents, with thicker iceberg tracks similar to, but eastward of, those of thinner icebergs. Amigosberg calved from the southern Larsen C shelf, and is likely the thinnest iceberg of the study group. It drifted considerably west of the others, into the Bransfield Strait region, and passed between Elephant Island and Clarence Island and then well to the west of South Georgia on a more north-northeasterly track. Another repetitive pattern, with differences likely due to iceberg thickness, is the interaction with east–west-trending shoals along the eastern Peninsula shelf. These shoals extend eastward from islands or east–west-trending peninsulas along the Antarctic Peninsula (e.g. Jason Peninsula; Gipps Ice Rise). Long periods of iceberg groundings were observed at 66.5°S (southeast of Jason Peninsula), 68.5°S (Gipps Ice Rise) and 71°S (Dolleman Island). Based on the shoal and coastal-shelf interactions (Figs 2 and 3), the thickest icebergs of the study set were A43B and A22A; the thinnest were Amigosberg and A43A. However, inferred iceberg thickness was not a good predictor of eventual drift path; both A43B and Amigosberg passed west of South Georgia Island.

Deeper ocean-current controls on the icebergs also appear to be highly repetitive (e.g. in the region northwest
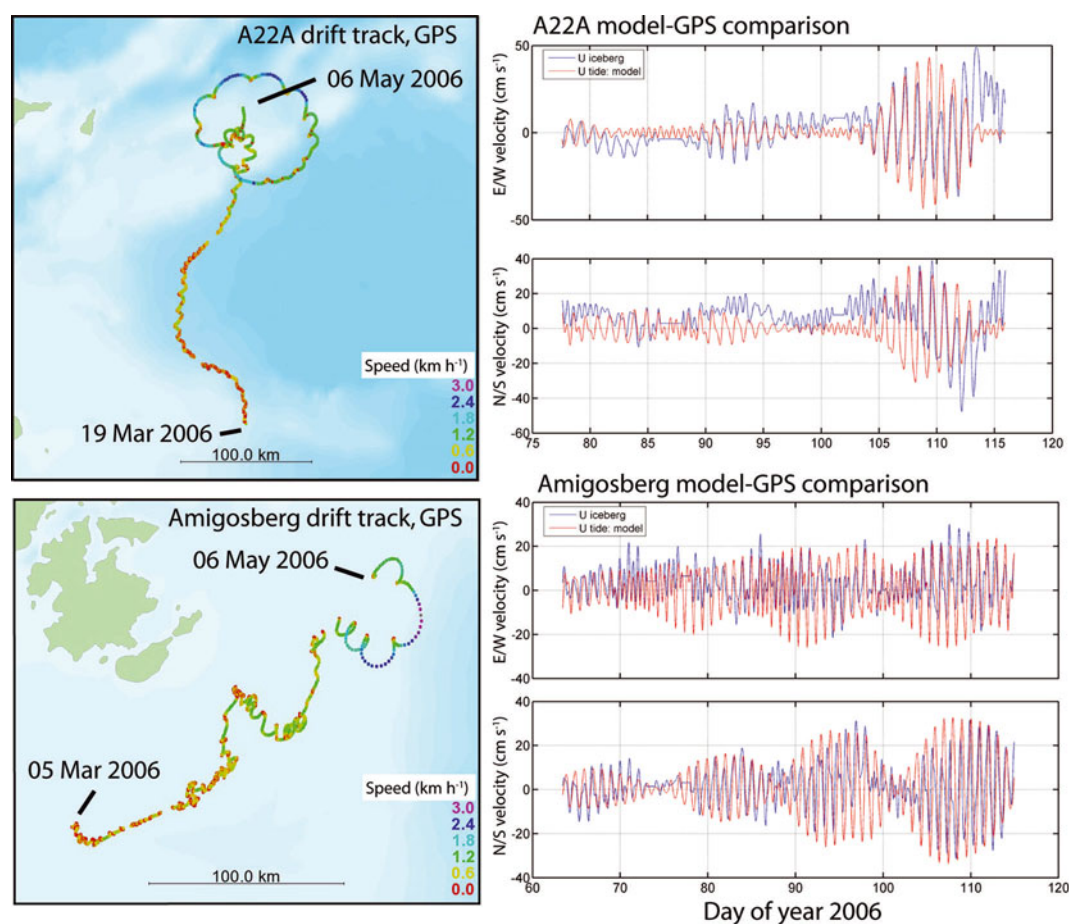
Fig. 4. Comparison of GPS positions and mean velocity uplinked from AMIGOS units on A22A and Amigosberg (UK211), with modeled motion based on tidal slopes and iceberg drift (Padman and others, 2002). Model velocities do not include any net drift; the multi-day deviation from zero for the observed iceberg drift is a measure of mean drift.

of Orcadas island near 47° W). In this area, three of the icebergs underwent large gyre-like motions, all of them having ∼80 km diameter 'orbits'. Further east, the iceberg tracks were sinuous, with similarly located meanders. A remarkable coincidence of drift tracks occurs northwest of South Georgia, where three of the studied icebergs, Amigosberg, A43B and A22A, all drift within a few kilometers of the same narrow path near 52° S, 43° W, two of them for a distance of >200 km (Figs 2 and 3; A43B could not be followed farther because of break-up). This may be related to a deep escarpment with the same trend along the eastern side of Maurice Ewing Bank at 2000–3000 m water depth (Fig. 3). The implication is that the topography may be directing a narrow convergence of deep ocean flow through geostrophism (Thorpe and others, 2002).

Daily motion of icebergs is a combination of iceberg rotation (requiring ∼2–20 days to complete) and cycloidal drift with a daily or twice-daily period of oscillation, which we observed with the AMIGOS GPS units on Amigosberg and A22A (Fig. 4). Drift speeds during the daily cycle averaged 1–2 km h^{-1}. A comparison of daily drift velocities and a tidal model is shown at right in Figure 4. Ocean tidal currents were evaluated using the Antarctic Peninsula barotropic tide model, version 04.01 (AntPen04.01). This model is constructed on a 1/30° × 1/60° (∼2 km) grid, and calculates the tides as the solution to the depth-integrated shallow-water wave equations (Robertson and others, 1998), forced at the open boundaries by the CATS02.01 tide model

(Padman and others, 2002). A simple scaling analysis of the force balance for a freely drifting iceberg suggests that the principal force balance is between sea surface slope and Coriolis, and that lateral and basal stresses due to currents are comparatively small (but the resulting drift accumulates on timescales longer than 1 day). Barotropic tide models, which are also dominated by the balance between the surface pressure gradient and Coriolis, should therefore adequately represent the iceberg motion (personal communication from L. Padman, 2007). Figure 4 illustrates that this is largely the case for the two AMIGOS-bearing icebergs. Iceberg drift amplitude and timing closely mimics the tidally driven model, with amplitudes varying as tidal amplitudes vary in the spring-to-neap tidal pattern. Errors in the comparison are in part due to the location of the AMIGOS units near the edge of the icebergs, i.e. not near the center of iceberg rotation. Timing and amplitude strongly support the model assumptions that current drift stress is minor (but noticeable as the non-zero mean for multi-day periods for the icebergs), and that the majority of motion on a daily basis is due to tidal tilt of the ocean surface.

Iceberg edge and surface structures from photography

Hand-held photography from ship-borne, airborne, in situ and astronaut viewing perspectives illustrates a number of iceberg physical properties and processes (Fig. 5). As part of the field preparation and field expedition landings, we examined the edges and surfaces of Amigosberg, A22A and
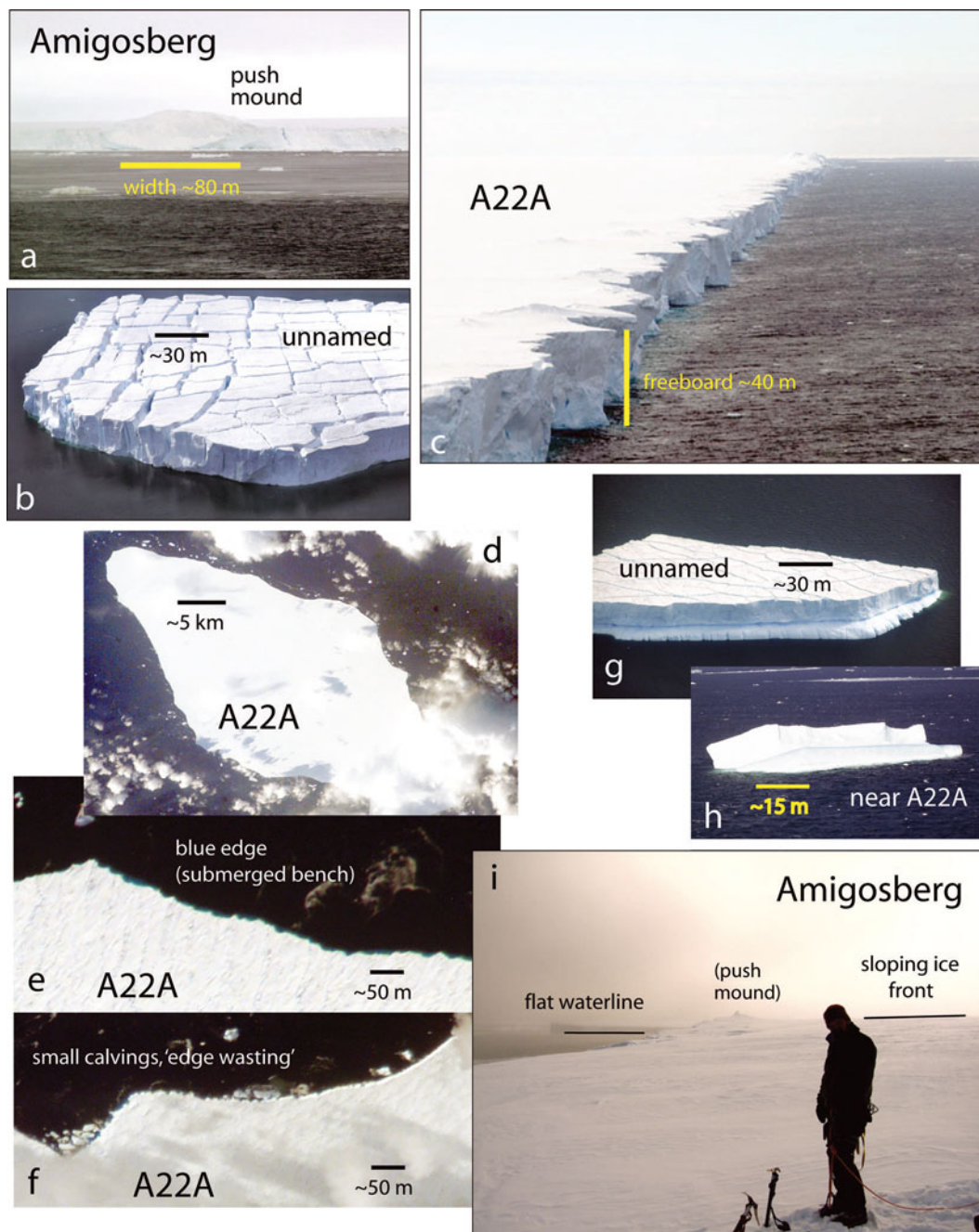
Fig. 5. Ship-borne, aerial, surface and ISS hand-held photographs of icebergs showing several aspects of iceberg processes: (a) large push mound on the edge of Amigosberg, viewed from the *Irizar*; (b) aerial view of surface fracturing typical of small icebergs in open-water region near Marambio; (c) aerial view of cavernous erosion of the A22A edge in the Scotia Sea; (d) ISS hand-held near-nadir view of A22A, 31 May 2006; (e) ISS image of edge of A22A, 31 May, showing blue perimeter indicating submerged 'bench' feature; (f) ISS image of same edge area on 7 June showing multiple small calvings; (g, h) ice 'benches' emergent on small icebergs resulting from waterline melting; and (i) in situ photograph of Amigosberg edge in Weddell Sea showing 'berm' bending of ice margin. ISS images are from 31 May and 7 June 2006; image identifier numbers are ISS015-E-10122, -10118 and -11254, for (d), (e) and (f) respectively.

numerous smaller icebergs near Marambio station. Iceberg freeboard faces were vertical and relatively smooth in cold-water regions (i.e. south of the sea-ice edge; Fig. 1c) but exhibited cavernous erosion at the waterline in open ocean areas north of the ice edge (Fig. 5b). Edges of all larger icebergs (>3 km across) showed sections that appeared crushed, extending along the ice edge for distances of a few meters to hundreds of meters, and forming ridges extending 5–15 m above the iceberg edge (Fig. 5a, center). These areas have been termed 'push mounds' in past studies, and are observed to result from iceberg–iceberg collisions

(MacAyeal and others, 2008). Icebergs smaller than ~1 km in shortest horizontal dimension, and in sea-ice-free water, showed evidence of flexure (Fig. 5b and g), presumably from long-period ocean swell (Goodman and others, 1980; Kristensen and others, 1982). However, icebergs larger than ~1 km in smallest horizontal dimension in general had unfractured interiors at the scale of visible observation from aircraft and hand-held space photographs (Fig. 5b, d and i), and were only sparsely fractured within a few hundred meters of their edges. Waterline ice profiles were observed from the iceberg edges and from aircraft. These were visible

in clear sea water to about 10 m depth. In sea-ice-covered regions the waterline profiles were near-vertical, and continuous with the vertical freeboard face. However, in areas north of the sea-ice edge, distinct 'bench' structures were observed, both below the waterline and emergent above it (Fig. 5e, g and h; the 'bench' term used here and in Scambos and others (2005) is similar to the terms 'ram', 'spur' or 'apron' used in oceanographic studies). Waterline erosion led to 'spalling', or above-waterline calving, resulting in tilting of smaller icebergs as they compensated for above-waterline mass loss (see Scambos and others, 2005). At a larger scale, hand-held images from the ISS showed evidence of below-waterline benches and regions of multiple edge-parallel small iceberg calvings (Fig. 5d–f). In contrast, surface observations of the margin of Amigosberg during the installation of the AMIGOS unit (Fig. 5i) indicated a pattern of bending of the outer $\sim$500 m of ice edge towards the waterline. At the time of the visit (3–4 March 2006), Amigosberg was at 65.4°S, well south of the sea-ice edge. This 'head-down' (or 'berm' (Scambos and others, 2005)) bending of larger cold-water icebergs is opposite the bending of edges for large icebergs north of the sea-ice edge, but is a result of well-known bending forces resulting from the varying vertical gradients of pressure in ice versus water (e.g. Reeh, 1968). The profile near the Amigosberg ice edge is a low-relief berm at the perimeter of the iceberg (Fig. 5i; see also Scambos and others, 2005). The elevation change from the berm crest to the edge of the iceberg was estimated to be $\sim$4 m for Amigosberg, with the berm crest about 500 m from the ice edge (distance determined from hand-held GPS; crest determined visually).

Ice-core and snow-pit measurements

Firn temperature profile and firn density measurements collected during the AMIGOS installation at A22A on 19 March 2006 are shown in Figure 6. Firn temperature at the surface was –6.4°C (air temperature was –7.3°C). The temperature profile shows a strong warming trend with depth for the uppermost 1.5 m, to –1.2°C. Below that, the firn becomes colder with depth, the temperature dropping to –2.6°C at 5 m, and –15.1°C at 11 m. This lower temperature is significantly colder than the mean annual temperature for the northern Peninsula region, but just a few degrees higher than mean annual temperatures near the Ronne front (–17 to –25°C; see http://nsidc.org/data/thermap). Snow-pit measurements of firn density show a similar pattern, with low-density fresh snow on the surface, gradual densification with depth coupled with snow grain and snow structural indications of warm temperatures and past melt, and then lower-density snow at greater depths (Fig. 5, inset). At Amigosberg, on 4 March 2006, and near 64.5°S, drill cores to 3 m (drilled for ablation stake installations) showed a $\sim$60 cm layer of fresh snow underlain by coarse 'corn' snow with numerous melt layers to the bottom.

Calving styles and edge-wasting rates: MODIS satellite images

MODIS data for three of the study set icebergs (A38A, A38B and A43B) were used to identify three calving styles. 'Rift calvings' was the term applied to calvings resulting in large (>5 km^2) daughter icebergs. These were observed to occur by further fracturing of pre-existing rifts in the iceberg surface. In some cases, the rifts were inherited from structures formed in the parent ice-shelf environment (e.g.
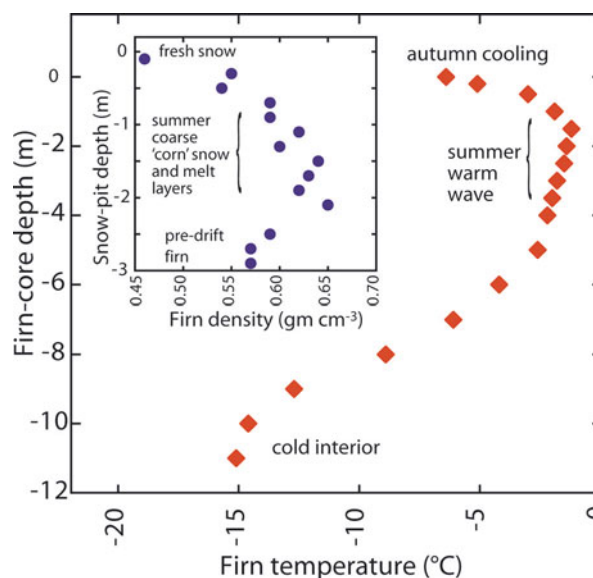

Fig. 6. Firn temperature from 11 m ice core taken at A22A during AMIGOS installation on 19 March 2006. Inset: firn-pit density on same date, adjacent to firn core. Temperature errors are ±0.5°C; firn density errors are ±0.03 g cm^{-3}. 'Pre-drift' refers to the period prior to the rapid northward movement of A22A beginning in early 2005.

A38A, A38B and A22A, and the Ronne Ice Shelf near Berkner Island). However, rifts also appeared in iceberg interiors where no visible fracture was previously apparent (in satellite images). The 'edge-wasting' calving style was observed to occur only in sea-ice-free water, and was characterized by small (<1 km wide) edge-parallel calvings in which the iceberg shrinks in area but the overall shape of the edge is approximately preserved. 'Rapid disintegration' is a process of myriad small calvings in rapid succession, sometimes in just one region of the iceberg (e.g. A43A in Fig. 7). True-color MODIS images and hand-held astronaut photographs indicate that surface melt ponding (A43B) is observed in some cases just before or during these rapid break-ups (Scambos and others, 2005, fig. 4). This calving pattern is very similar to the recent disintegrations of the Larsen B ice shelf in 2002 and the Wilkins Ice Shelf in 2008.

A series of MODIS satellite images of the two field-studied icebergs, A22A and Amigosberg, provide a record of area changes (Fig. 8). Using $\sim$35 images for each iceberg spanning the period of drift from sea-ice-covered areas to the region north of South Georgia Island, we measured iceberg area and perimeter length from projected imagery. In Figure 8 we plot the loss of area in square kilometers, and, in red (right axis), the area loss in hectares per kilometer of iceberg perimeter per day. The units of the right axis can be restated as units of 10 m d^{-1}, i.e. as a mean edge retreat rate, in the case of 'edge wasting'.

Iceberg area loss was minimal while the two icebergs were within the sea-ice edge. However, as soon as they entered open ocean water, a steady area loss began. Rates near the sea-ice edge were typically 1–2 ha km^{-1} d^{-1}, rising to 3–10 ha km^{-1} d^{-1} as the icebergs neared South Georgia Island. The A22A iceberg emerged briefly from the sea-ice edge in late austral summer 2006 but was then partially re-engulfed by sea ice as autumn growth of sea ice began. Edge loss rates were near-zero during this winter interval. Note that area loss ceased even for edges *not* within the sea-ice
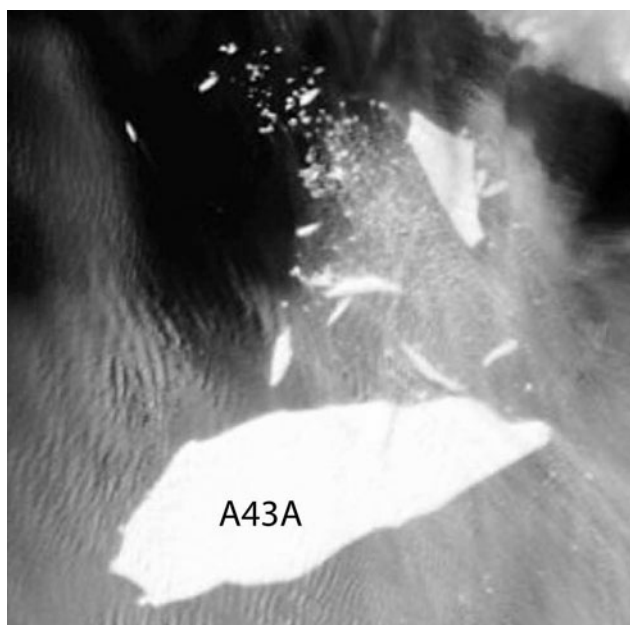
Fig. 7. MODIS image of A43A on 31 March 2005, showing rapid break-up after extensive summer surface melting. Image is 75 km on a side; location is near 50° S, 20°W. (Aqua MODIS image acquired 1530 UTC on 31 March 2005.)

Fig. 8. Area loss and edge-wasting rates during the northward drift of A22A and Amigosberg. Units for righthand axes are area (in hectares) per kilometer of iceberg perimeter per day. This is equivalent to 'meters per day edge retreat rate'. Note pause in rate of loss for A22A as winter sea-ice extent enveloped the iceberg. Note also rate increase after 7 November 2006 on Amigosberg, when in situ photographs of a firn pit showed evidence of water-saturated firn (see Figs 8 and 9). Date is decimal fraction of a year.

pack, implying that temperature, and not wave action alone, is a key factor in area loss. Typical open-water sea-surface temperatures in the areas of drift of A22A and Amigosberg ranged from –1.7°C at the ice edge to 3°C north and east of South Georgia Island at the northeast edge of the study region. While the general increase in edge-wasting rates with sea surface temperature is clear, the area loss measurements are noisy (and we have just two icebergs), so we did not attempt to determine a quantitative empirical relationship. However, it is clear that edge wasting is associated with ice-free surface water.

The rates of edge-wasting loss determined over the whole iceberg can be compared to the rates determined from uplinked images of the flag line near A22A (Fig. 1b and e). At A22A, seven flags were set out, starting from the AMIGOS tower unit and spaced 200 m apart to 1.2 km away. The installation (on 19 March 2006) was placed 3 km from the station. On 11 August, the outermost flag calved away. Given the estimated distance of 3 km to the original ice edge (±0.5 km), this represents an 'edge-wasting' calving rate of 1.8 ± 0.3 km in 145 days, i.e. a rate of $12.4\,\mathrm{m\,d^{-1}}$ (or $1.24\,\mathrm{ha\,km^{-1}\,d^{-1}}$ in the notation of Fig. 8). The next flag was removed on 22 August (11 days, equal to $18.2\,\mathrm{m\,d^{-1}}$ or $1.8\,\mathrm{ha\,km^{-1}\,d^{-1}}$). However, by 4 September, A22A was partially within the sea-ice edge, and remained in or adjacent to sea ice until 30 October. Two flags were then lost between 21 and 26 November (~300 m, in 22–27 days, or approximately 8–$18\,\mathrm{m\,d^{-1}}$). In early December, the AMIGOS station tower tipped and no further usable images of the flag line were retrieved.

An examination of the series of MODIS images used for Figure 8 measurements showed that the shape of the icebergs was similar image-to-image even as area loss rates began to increase north of the sea-ice edge. Area changes apparently occur via numerous small ice-edge calvings, near or below MODIS pixel size, 250 m. However, such events were recorded by the hand-held ISS photography (Fig. 5d–f).
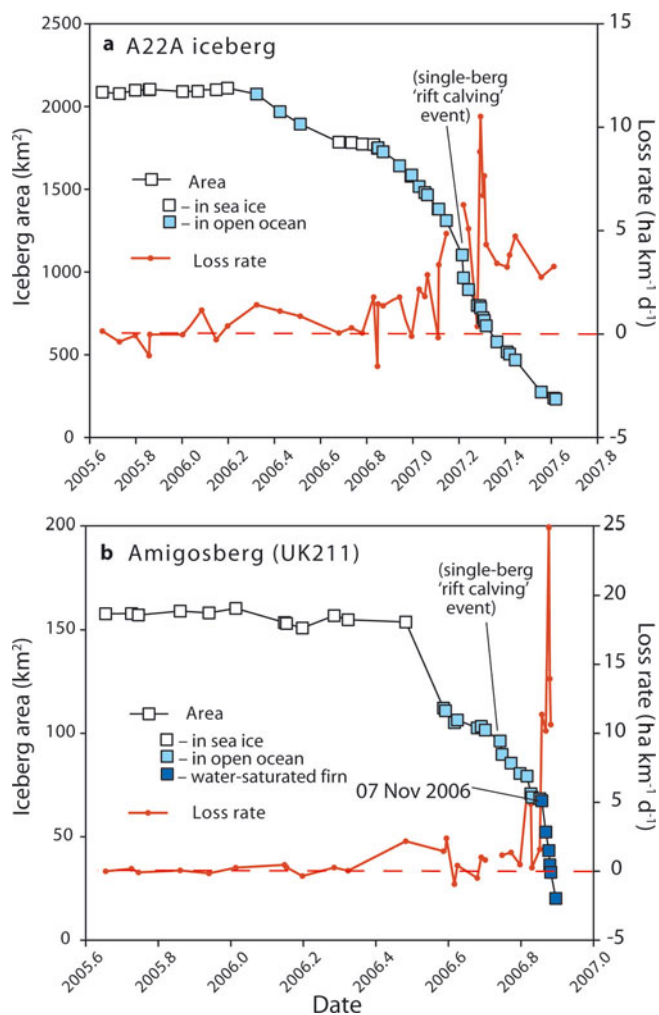
A few larger calving events followed pre-existing rifts in the icebergs, leading to sharp jumps in iceberg area. These are noted in Figure 8 and are not tracked by the red 'rate of area loss' line.

Rates jumped abruptly to $>10\,\mathrm{ha\,km^{-1}\,d^{-1}}$ ($>100\,\mathrm{m\,d^{-1}}$) for Amigosberg beginning with the 7–9 November 2006 MODIS image pair. The images reveal a number of near-simultaneous calvings, with calved icebergs spanning a range of sizes. A series of five MODIS images from 7 November through 23 November used for the area and perimeter measurements is shown in the upper half of Figure 9. Sequential, 'crumbling' calvings appear to be indicated. AMIGOS camera observations of the snow surface on the iceberg provide evidence for water saturation in the firn just prior to the rapid break-up (Fig. 8b; see following subsection). Amigosberg could not be tracked in MODIS after 23 November.

Observations from in situ AMIGOS units

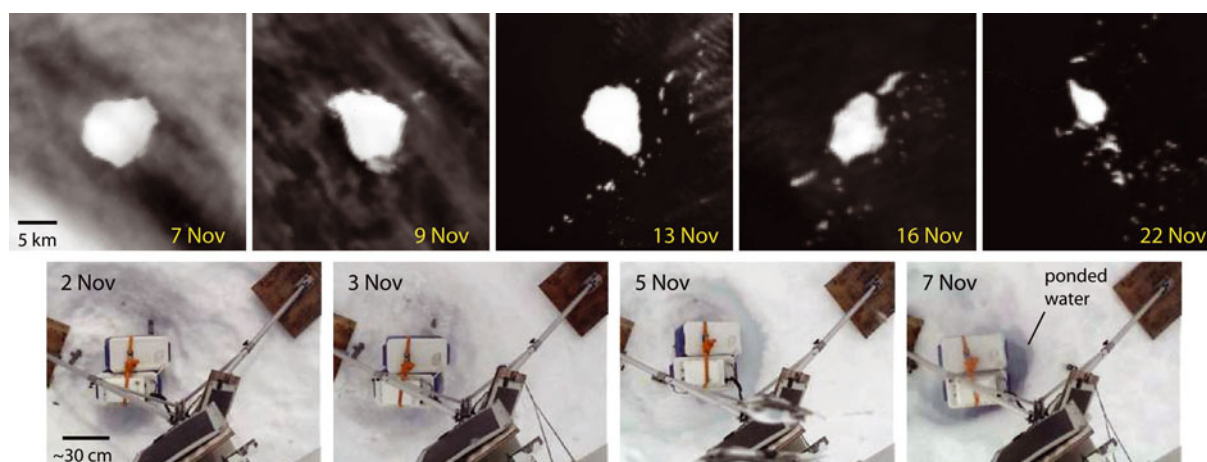A record of accumulation and ablation was extracted from ~60 AMIGOS camera images of each of the accumulation

Fig. 9. MODIS band 1 images of the late stages of break-up of Amigosberg (top), and firn-pit photographs from the AMIGOS unit in the days leading up to the rapid increase in break-up rate (bottom).

masts and ablation poles at Amigosberg and A22A (green line, Fig. 9). We compare these results with the hourly 1 m air temperatures recorded by the stations (red line), and extract degree-hours plots from the data (blue line; degree-hours is a running summation of number of hours spent above 0°C multiplied by the temperature in degrees). Both icebergs initially showed both accumulation and ablation periods in austral autumn, as temperatures gradually dropped. Cooling weather in mid-2006 led to greater net accumulation, and the lower solar panel at the Amigosberg station became buried, temporarily ending transmissions. During austral winter, the two icebergs remained within a few hundred kilometers of each other. The A22A station recorded 70 cm of accumulation, until austral spring warming beginning in early October brought higher ablation rates, and increased rainfall (noted as droplets upon the camera enclosure). Following this warm-up, 1 m of ablation occurred at A22A. By 10 October, ablation re-exposed the lower solar panel at Amigosberg and it resumed transmission.

Rates determined by a comparison of ablation and air temperature for both icebergs ranged between 1400 and 2700 degree-hours per meter of snow ablation. Extrapolating to the late stages of iceberg decay (two more weeks of melting occurred after the end of the ablation data in Fig. 10b), we estimate that ∼1 m of surface snow is melted and drained into the underlying firn by the late stages of iceberg break-up on Amigosberg. This implies a significant firn densification, a reduction in freeboard independent of basal melting, and increased refrozen melt in the subsurface.

An important result from the Amigosberg AMIGOS unit is the observation of ponded water just below the firn surface in the days just prior to an increase in rate of break-up. In Figure 8b, we show four images of a pit formed around the batteries during the ablation period (probably because the pit was filled with loose snow when the site was installed). Only white firn is present in the pit on 2 and 3 November 2006 (and in previous images). A pale-bluish tint is visible in the pit on 5 November, and on 7 November a darker-blue region is visible. We interpret this as a small pool of meltwater, indicating shallow firn saturation with water. As noted above, an abrupt increase in calving rate and a change in calving style was observed in satellite imagery immediately after this time. The Amigosberg AMIGOS unit tipped over shortly after 7 November, and transmission ceased on

23 November. The AMIGOS unit on A22A went silent on 22 January 2007.

Ice-thickness changes: ICESat freeboard data

Three elevation profiles from separate ICESat data acquisition periods, from 4 November 2004, 13 March 2006 and 10 November 2006, provide near-repeat freeboard measurements across the same region of the A22A iceberg (Fig. 10); this is a remarkable coincidence considering drift and rotation of the iceberg, and spacing of ICESat tracks. An earlier study of ICESat data at laser-profile crossing points on the A38A and A38B icebergs indicated freeboard changes were small while the icebergs remained in the Weddell Sea (∼1 ± 0.7 m freeboard change per year; Scambos and others, 2005; see also Jansen and others, 2007). For A22A, a comparison of a 15.5 km section of the central part of the iceberg (Fig. 9, lower panels) indicates net freeboard changes were near-zero within error (∼±1.3 m) over a 17 month period of northward drift, during which time the iceberg moved from near the Ronne Ice Shelf front (73.0° S) to the edge of the sea ice (62.2° S). In the following 8 months, the iceberg lost 7.8 ± 1.5 m of freeboard. Values are computed by subtracting the mean for the entire 15.5 km profile section; results were within 0.1 m when computed by subtracting individual elevation points closest to the same distance from the rift feature in profiles. We note that this higher rate of freeboard loss occurred without an extended period of grounding, invoked to explain rapid loss of A38B freeboard (which grounded northeast of South Georgia Island; Jansen and others, 2007).

As noted above, this freeboard change is a combination of the effects of basal melting and firn densification. For the second pair of ICESat tracks (13 March 2006 and 10 November 2006), the AMIGOS on board A22A made continuous observations of snowfall and melting (Fig. 9), indicating a net of about 35 ± 5 cm ablation. Thus 7.5 m of freeboard loss may be attributed to a combination of basal melting and firn compaction below the ∼3 m level of the base of the ablation poles. Although A22A survived until November 2007, no further ICESat tracks (none with surface data) crossed the iceberg. However, we note that rates of ablation were quite rapid (0.7 m month^{-1}) toward the end of the A22A AMIGOS transmission period, and freeboard would likely have been reduced by a few meters due to these processes in the late
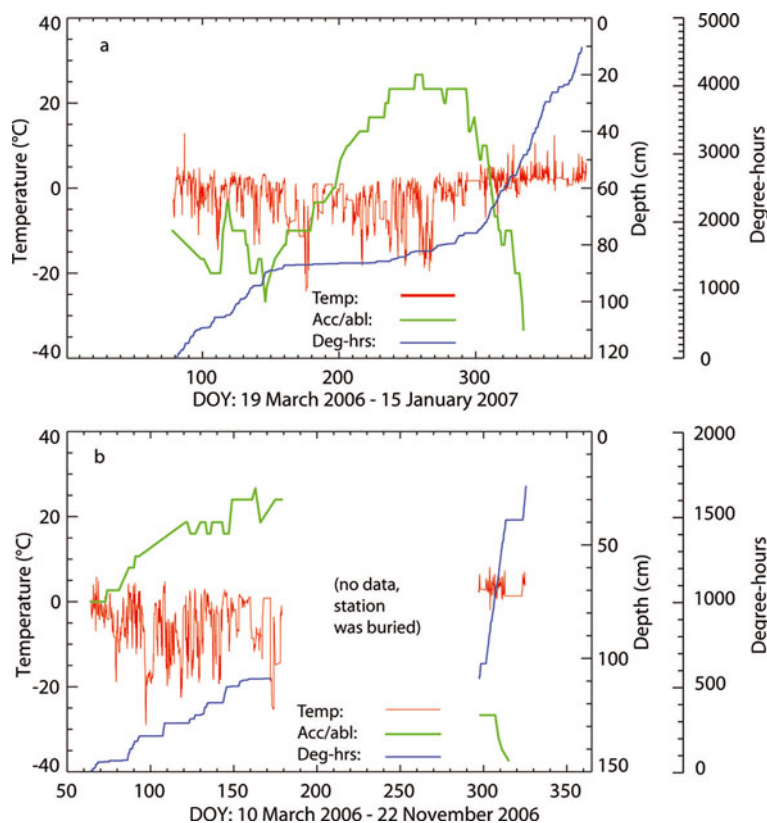
Fig. 10. Air temperature, accumulation–ablation and cumulative degree-hours from AMIGOS units on A22A (a) and Amigosberg (b). Day-of-year (DOY) axis is referred to 1 January 2006. Depth axis refers to a mark on the accumulation/ablation masts, set initially 75 cm above snow level.

stages of the iceberg's break-up. Firn densification due to surface melt may partly explain the very rapid freeboard loss in A38B (as it was grounded through a summer season northeast of South Georgia). Scambos and others (2005) observed a ∼10 m loss in 4.5 months; a more careful two-dimensional melt model study, tied to ICESat observations (Jansen and others, 2007), showed a ∼8 m loss; both these measurements are nearly twice the rate of A22A.

Iceberg-firn changes and surface melting from scatterometry

Microwave scatterometry of the upper firn on icebergs changed rapidly as the icebergs drifted north of the tip of the Peninsula and into a warmer climate (Fig. 11). The pattern of backscatter change through time follows that of facies changes with elevation and melt-season length on ice sheets (Fahnestock and others, 1993; Long and others, 2002). Backscatter levels are initially low to moderate when icebergs are near the ice shelves from which they originated, depending upon the accumulation, mean temperature, and melt season length on the source ice shelf. Dry snow on the icebergs is moderately radar-absorbing, with backscatter values near –5 to –10 dB (σ^0). As northward drift progresses, the icebergs encounter warmer summer conditions, and experience more extensive melt. Melt events are characterized by large and abrupt reductions in backscatter, typically 10–15 dB lower than the initial dry snow. Refreezing of this melt as it percolates into colder underlying firn creates rough ice layers and other features within the firn, increasing backscatter (Scambos and others, 2003; Kunz and Long, 2006). This leads to rising winter backscatter levels after each of the first few warmer summer periods the icebergs encounter. As melt

season and melt intensity increases, the underlying firn becomes saturated with refrozen ice. Backscatter levels peak near –2 dB. As melt continues, specular reflection of the increasingly smooth and icy upper surface leads to reduced backscatter. For three of the study icebergs, rapid disintegration occurred as backscatter levels of refrozen surfaces approached those of the melt events, i.e. –15 to –20 dB (Fig. 12). In two of these cases, we found evidence of ponded water or saturated firn occurring just prior to break-up: on Amigosberg, firn ponding in a snow pit; and on A43B, large surface ponds in ISS photographs and MODIS images (see Scambos and others, 2005). On A43A (Fig. 6), a break-up pattern similar to the A43B and Amigosberg break-ups was seen at the end of a summer season at relatively low latitude.

DISCUSSION AND CONCLUSIONS

Rapid northward drift of large tabular icebergs causes them to encounter rapidly increasing mean air and ocean temperatures, in excess of the stability limit inferred for ice shelves (see Vaughan and Doake, 1996; Morris and Vaughan, 2003). Monitoring of the evolution and break-up of the icebergs indicates that two processes, termed here 'edge wasting' and 'rapid disintegration', are the primary causes of mass loss and break-up, and occur only in climates outside the sea-ice edge (and cease if the ice edge re-engulfs the iceberg (e.g. Fig. 7, A22A pattern)). A consideration of these processes, and the backscatter changes on iceberg surfaces, leads us to propose several predictive, semi-quantitative tests for stability of floating ice plates in changing climates.

The observation of waterline erosion, the formation of 'benches', and the onset of significant edge wasting of
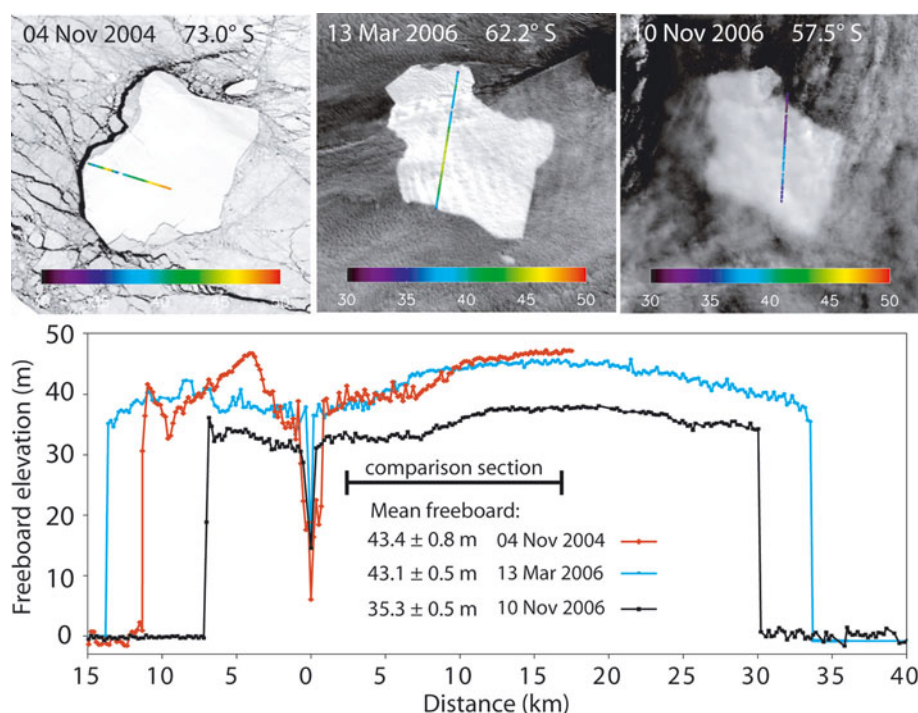
Fig. 11. Top: ICESat elevation profile locations plotted over MODIS images of A22A acquired near the time of overpass (projection and image orientation changes among the three images). Images are all 100 km on a side. For the 10 November 2006 profile-image pair, GPS data from the AMIGOS station show that the iceberg drifted 8 km northeast between the MODIS image (1235 UTC) and the ICESat overpass (2232 UTC). The other two image-overpass pairs were within 4 hours. Bottom: Elevation profiles show in detail the mean changes in freeboard. Profiles are aligned on a rift that all three profiles crossed. 'Comparison section' is a 15 km long region adjacent to the rift in the iceberg interior used for determining mean freeboard changes over time.

icebergs only after drifting into ice-free, above-freezing water implies that waterline erosion plays a significant role in ice-shelf or ice-tongue retreat. In this scenario, loss of a sea-ice cover leads to solar warming of surface water. Waterline erosion causes above-waterline 'spalling' of the freeboard firn, leaving a below-waterline 'bench' of ice. This bench begins to stress the ice plate, lifting the ice edge and eventually forming an upward-propagating bottom crevasse. Scambos and others (2005) noted the 'rampart-and-moat' edge profile from ICESat data is probably caused by this pre-fracture flexing. Modeling of this process in that study confirmed that submerged 20–40 m protrusions, or 'benches', formed by waterline erosion, would lead to the ICESat elevation profile as observed. The ISS image series captures an edge-wasting event in detail (Fig. 4d–f), and there is abundant evidence of the process from other aerial, shipboard and in situ images. As the bench increases, stress builds until bottom calving releases a secondary iceberg, causing the main iceberg (or ice tongue or ice shelf) to shrink in area. Edge-wasting rates are typically a few meters to a few tens of meters per day in the Scotia Sea and South Atlantic, where water temperatures are –1 to 3°C (Fig. 7). This rate is equivalent to the most rapid ice-tongue flow rates observed in Greenland or the Antarctic (Joughin and others, 2004; Rignot and others, 2004; Howat and others, 2007; Hulbe and others, 2008); ice tongues in solar-warmed open water that move at less than this rate will likely retreat by the edge-wasting process (e.g. during a few months in late summer). Indeed, southeastern Greenland ice tongues are observed to retreat primarily in spring/summer by a mixture of large rift events and numerous <1 km calvings (Howat and others, 2007), and these events are followed by an acceleration of ice flow and a change to negative mass balance. Thus we offer a potentially predictive tool for ice-tongue retreat based on observation of ice-free conditions at the ice front, scaling with surface water temperature. The edge-wasting model points to a high sensitivity of exposed, sea-ice-free, floating ice fronts; relatively little warming of the surface water is required, and the surface water layer need not be very thick.

Basal melt of icebergs increases rapidly with northward drift, as inferred from freeboard measurements. However, a significant fraction of this freeboard reduction can be due to firn densification from surface melt and percolation in the latest stages of decay. Nevertheless, thinning rates increase rapidly as the iceberg transitions from the Weddell Sea to the Scotia Sea and southern South Atlantic areas. Rates within the Weddell Sea are small, likely 0–10 m a^{-1}, based on our freeboard changes. Even with a correction for densification, basal melt rates in the Scotia Sea and South Atlantic Ocean are ~100 m a^{-1}. It is still unclear if a critical minimum iceberg thickness (or minimum shelf thickness) is a factor in iceberg/ice-shelf disintegration (e.g. Shepherd and others, 2003).

Our study strongly supports the theory that accumulated meltwater on an iceberg surface (or ice-shelf or ice-tongue surface), or stored water within porous firn, has a major effect on iceberg/ice-shelf stability. The effect of this water is presumably increased fracture penetration, as outlined by Weertman (1973), Scambos and others (2003) and Van der Veen (2007). Rates of edge wasting increased by nearly an order of magnitude on Amigosberg after the observation of saturated firn. A similar large increase in calving rate was observed for A43B after ponds were imaged on its surface (Scambos and others, 2005), and for A43A after extensive
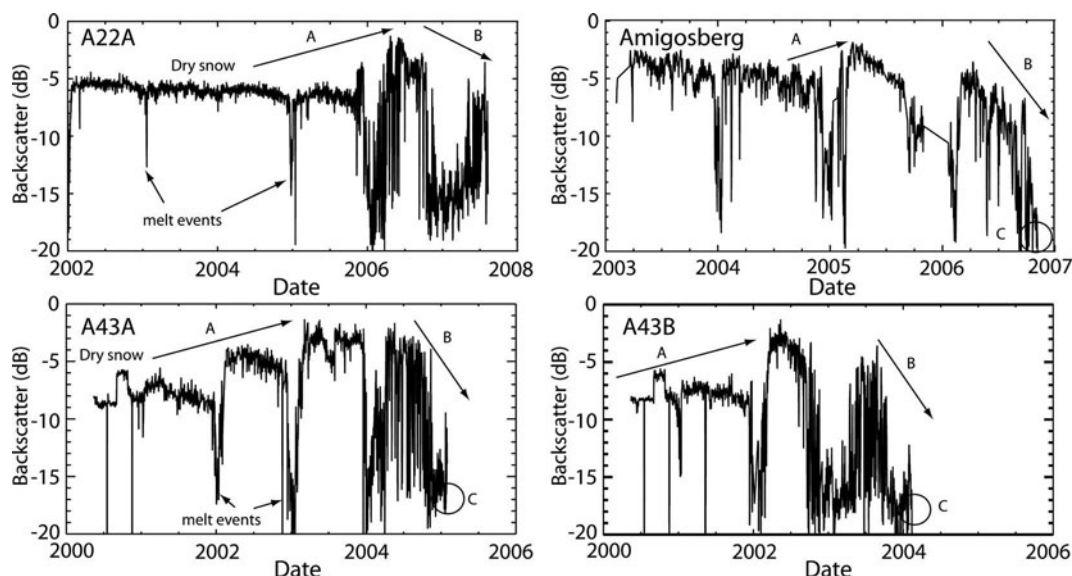
Fig. 12. Backscatter evolution of four of the icebergs in this study. Melt events are indicated by large abrupt drops in backscatter. Patterns of firn evolution with increasing melt are: (A) increasing backscatter after extended melt events in early evolution; (B) decreasing backscatter after refreeze as melt events become longer and more intense due to saturation of melt layers and specular reflection; and (C) rapid disintegration event as refrozen backscatter levels reach ~15 dB. A22A did not disintegrate during the period of observation. Amigosberg was not tracked for backscatter until March 2006. Backscatter 'events' of middle and late 2000 for A43A and A43B are sensor artifacts.

melting and surface backscatter changes (Figs 6 and 12). These retreat rates are equivalent to hundreds of meters per day of edge retreat, a rate far beyond any observed ice flow, but similar in rate and calving style to the catastrophic retreat rates of the Larsen B and Larsen A events. Wilkins Ice Shelf experienced similar, partial, catastrophic calvings in 1998 (Scambos and others, 2000), and has been observed to have water-saturated firn with only isolated surface ponds (Vaughan and others, 1993).

Icebergs are significantly flexed by ocean swell, but the degree to which this can induce large-scale fracturing appears to be linked to iceberg size, and therefore must depend on the wavelength of the ocean current. Given the effects on ~1–2 km icebergs noted here (Fig. 4c and g), it is worth investigating whether smaller effects may occur on larger icebergs, or, more importantly, on ice shelves with exposure to ocean swell. The effect of swell has been implicated in a very large iceberg break-up in the Ross Sea region (MacAyeal and others, 2006). We note that free-drifting icebergs of this study are exposed to ocean swell continuously, so rapid, disintegrating break-up by swell alone is unlikely. However, it is possible that long-period swell may act as a trigger for ice-shelf break-up once firn saturation with meltwater has occurred.

Changes in backscatter from icebergs as they drift and eventually break up offer a path to prediction of when ice shelves are likely to disintegrate via the 'rapid disintegration' process. Scambos and others (2003) identified a similar pattern spatially among ice shelves with varying melt-season lengths, and the observation of a similar trend on icebergs over time shows that the trend is evolutionary with increasing melt. Long-term observations of ice-shelf backscatter should allow an evaluation of where in the firn evolution pattern (or snow facies series) the shelf surface is. Continuous monitoring of climate and backscatter over ice shelves would permit the time of surface water saturation, and therefore rapid disintegration, to be approximately forecast.

REFERENCES

Doake, C.S.M., H.F.J. Corr, H. Rott, P. Skvarca and N.W. Young. 1998. Breakup and conditions for stability of the northern Larsen Ice Shelf, Antarctica. *Nature,* **391**(6669), 778–780.

Early, D.S. and D.G. Long. 2001. Image reconstruction and enhanced resolution imaging from irregular samples. *IEEE Trans. Geosci. Remote Sens.,* **39**(2), 291–302.

Fahnestock, M., R. Bindschadler, R. Kwok and K. Jezek. 1993. Greenland ice sheet surface properties and ice dynamics from ERS-1 SAR imagery. *Science,* **262**(5139), 1530–1534.

Ferrigno, J.G. and W.G. Gould. 1987. Substantial changes in the coastline of Antarctica revealed by satellite imagery. *Polar Rec.,* **23**(146), 577–583.

Gladstone, R. and G.R. Bigg. 2002. Satellite tracking of icebergs in the Weddell Sea. *Antarct. Sci.,* **14**(3), 278–287.

Goodman, D.J., P. Wadhams and V.A. Squire. 1980. The flexural response of a tabular ice island to ocean swell. *Ann. Glaciol.,* **1**, 23–27.

Haran, T.M., M.A. Fahnestock and T.A. Scambos. 2002. De-striping of MODIS optical bands for ice sheet mapping and topography. [Abstract C12A-1003.] *Eos,* **88**(47), Fall Meet. Suppl., F317.

Howat, I.M., I.R. Joughin and T.A. Scambos. 2007. Rapid changes in ice discharge from Greenland outlet glaciers. *Science,* **315**(5818), 1559–1561.

Hulbe, C., T. Scambos, T. Youngberg and A. Lamb. In press. Patterns of glacier response to disintegration of the Larsen B ice shelf, Antarctic Peninsula. *Global Planet. Change.*

Jansen, D., M. Schodlok and W. Rack. 2007. Basal melting of A-38B: a physical model constrained by satellite observations. *Remote Sens. Environ.,* **111**(2–3), 195–203.

Joughin, I., W. Abdalati and M.A. Fahnestock. 2004. Large fluc-tuations in speed of Jakobshavn Isbræ, Greenland. *Nature,* **432**(7017), 608–610.

Kristensen, M., V.A. Squire and S.C. Moore. 1982. Tabular icebergs in ocean waves. *Nature,* **297**(5868), 669–671.

Kunz, L.B. and D.G. Long. 2006. Melt detection in Antarctic ice-shelves using spaceborne scatterometers and radiometers. *IEEE Trans. Geosci. Remote Sens.,* **44**(9), 2461–2469.

Long, D.G., J. Ballantyne and C. Bertoia. 2002. Is the number of Antarctic icebergs really increasing? *Eos,* **83**(42), 469, 474.

MacAyeal, D.R., T.A. Scambos, C.L. Hulbe and M.A. Fahnestock. 2003. Catastrophic ice-shelf break-up by an ice-shelf-fragment-capsize mechanism. *J. Glaciol.,* **49**(164), 22–36.

MacAyeal, D.R. *and 13 others.* 2006. Transoceanic wave propa-gation links iceberg calving margins of Antarctica with storms in tropics and Northern Hemisphere. *Geophys. Res. Lett.,* **33**(17), L17502. (10.1029/2006GL027235.)

MacAyeal, D.R., M.H. Okal, J.E. Thom, K.M. Brunt, Y.-J. Kim and A.K. Bliss. 2008. Tabular iceberg collisions within the coastal regime. *J. Glaciol.,* **54**(185), 371–386.

Morris, E.M. and D.G. Vaughan. 2003. Spatial and temporal variation of surface temperature on the Antarctic Peninsula and the limit of viability of ice shelves. *In* Domack, E., A. Leventer, A. Burnett, R.A. Bindschadler, P. Convey and M. Kirby, *eds. Antarctic Peninsula climate variability: historical and paleo-environmental perspectives.* Washington, DC, American Geo-physical Union, 61–68. (Antarctic Research Series 79.)

Padman, L., H.A. Fricker, R. Coleman, S. Howard and L. Erofeeva. 2002. A new tide model for the Antarctic ice shelves and seas. *Ann. Glaciol.,* **34**, 247–254.

Reeh, N. 1968. On the calving of ice from floating glaciers and ice shelves. *J. Glaciol.,* **7**(50), 215–232.

Rignot, E., G. Casassa, P. Gogineni, W. Krabill, A. Rivera and R. Thomas. 2004. Accelerated ice discharge from the Antarctic Peninsula following the collapse of Larsen B ice shelf. *Geophys. Res. Lett.,* **31**(18), L18401. (10.1029/2004GL020697.)

Robertson, R., L. Padman and G.D. Egbert. 1998. Tides in the Weddell Sea. *In* Jacobs, S.S. and R.F. Weiss, *eds. Ocean, ice and atmosphere: interactions at the Antarctic continental margin.* Washington, DC, American Geophysical Union, 341–369. (Antarctic Research Series 75.)

Ross, R., M. Okal, J. Thom and D. MacAyeal. 2004. Automatic, satellite-linked 'webcams' as a tool in ice-shelf and iceberg research. [Abstract C43C-0236]. *Eos,* **85**(46), Fall Meeting Suppl.

Rott, H., W. Rack, T. Nagler and P. Skvarca. 1998. Climatically induced retreat and collapse of northern Larsen Ice Shelf, Antarctic Peninsula. *Ann. Glaciol.,* **27**, 86–92.

Rott, H., W. Rack, P. Skvarca and H. De Angelis. 2002. Northern Larsen Ice Shelf, Antarctica: further retreat after collapse. *Ann. Glaciol.,* **34**, 277–282.

Scambos, T.A., C. Hulbe, M. Fahnestock and J. Bohlander. 2000. The link between climate warming and break-up of ice shelves in the Antarctic Peninsula. *J. Glaciol.,* **46**(154), 516–530.

Scambos, T., C. Hulbe and M. Fahnestock. 2003. Climate-induced ice shelf disintegration in the Antarctic Peninsula. *In* Domack, E.W., A. Burnett, A. Leventer, P. Conley, M. Kirby and R. Bindschadler, *eds. Antarctic Peninsula climate variability: a historical and paleoenvironmental perspective.* Washington, DC, American Geophysical Union, 79–92. (Antarctic Research Series 79.)

Scambos, T.A., J.A. Bohlander, C.A. Shuman and P. Skvarca. 2004. Glacier acceleration and thinning after ice shelf collapse in the Larsen B embayment, Antarctica. *Geophys. Res. Lett.,* **31**(18), L18402. (10.1029/2004GL020670.)

Scambos, T., O. Sergienko, A. Sargent, D. MacAyeal and J. Fastook. 2005. ICESat profiles of tabular iceberg margins and iceberg break-up at low latitudes. *Geophys. Res. Lett.,* **32**(23), L23S09. (10.1029/2005GL023802.)

Shepherd, A., D. Wingham, T. Payne and P. Skvarca. 2003. Larsen ice shelf has progressively thinned. *Science,* **302**(5646), 856–859.

Skvarca, P. and M.J. García. 1993. Deriva del témpano tabular Filchner 1986A. *In Segundas Jornadas de Comunicaciones sobre Investigaciones Antárticas.* Buenos Aires, Consejo Nacional de Investigaciones Cientificas y Tecnicas. Instituto Antartico Argen-tino, 105–109.

Squire, V.A. 2007. Of ocean waves and sea-ice revisited. *Cold Reg. Sci. Technol.,* **49**(2), 110–133.

Swithinbank, C., P. McClain and P. Little. 1977. Drift tracks of Antarctic icebergs. *Polar Rec.,* **18**(116), 495–501.

Thomas, R.H. 2004. Force-perturbation analysis of recent thinning and acceleration of Jakobshavn Isbræ, Greenland. *J. Glaciol.,* **50**(168), 57–66.

Thorpe, S.E., K.J. Heywood, M.A. Brandon and D.P. Stevens. 2002. Variability of the southern Antarctic Circumpolar Current front north of South Georgia. *J. Mar. Systems,* **37**(1–3), 87–105.

Van der Veen, C.J. 2007. Fracture propagation as means of rapidly transferring surface meltwater to the base of glaciers. *Geophys. Res. Lett.,* **34**(1), L01501. (10.1029/2006GL028385.)

Vaughan, D.G. and C.S.M. Doake. 1996. Recent atmospheric warming and retreat of ice shelves on the Antarctic Peninsula. *Nature,* **379**(6563), 328–331.

Vaughan, D.G., D.R. Mantripp, J. Sievers and C.S.M. Doake. 1993. A synthesis of remote sensing data on Wilkins Ice Shelf, Antarctica. *Ann. Glaciol.,* **17**, 211–218.

Weertman, J. 1973. Can a water-filled crevasse reach the bottom surface of a glacier? *IASH Publ.* 95 (Symposium at Cambridge 1969 – *Hydrology of Glaciers*), 139–145.

Wordie, J.M. and S. Kemp. 1944. Observations on certain Antarctic icebergs. *Polar Times,* **18**, 1–5.